Topology, Connectivity, and Electronic Structure of *C* and *B* Cages and the Corresponding Nanotubes

F. E. Leys,[†] C. Amovilli,*[,‡] and N. H. March[†,§]

Department of Physics, University of Antwerp (RUCA), Groenenborgerlaan 171 B-2020 Antwerpen, Belgium, Dipartimento di Chimica e Chimica Industriale, Università di Pisa, Via Risorgimento 35, 56126 Pisa, Italy, and Oxford University, Oxford, England

Received September 21, 2002

After a brief discussion of the structural trends which appear with an increasing number of atoms in *B* cages, a one-to one correspondence between the connectivity of *B* cages and *C* cage structures will be proposed. The electronic level spectra of both systems from Hartree−Fock calculations is given and discussed. The relation of curvature introduced into an originally planar graphitic fragment to pentagonal "defects" such as are present in buckminsterfullerene is also briefly treated. A study of the structure and electronic properties of *B* nanotubes will then be introduced. We start by presenting a solution of the free-electron network approach for a "model boron" planar lattice with local coordination number 6. In particular the dispersion relation $E(\mathbf{k})$ for the π-electron bands, together with the corresponding electronic Density Of States (DOS), will be exhibited. This is then used within the zone-folding scheme to obtain information about the electronic DOS of different nanotubes obtained by folding this model boron sheet. To obtain the self-consistent potential in which the valence electrons move in a nanotube, "the March model" in its original form was invoked, and the results are reported for a carbon nanotube. Finally, heterostructures, such as BN cages and fluorinated buckminsterfullerene, will be briefly treated, the new feature here being electronegativity difference.

I. BACKGROUND AND OUTLINE

The continuing usefulness of models of π-electrons in conjugated systems, for example that of Hückel,[1] testifies to the importance of geometry and connectivity in determining electronic structure. There has, indeed, been renewed interest in this area, due to the potential for technology of nanostructures.[2]

Therefore, in the present study of *C* and *B* cages, and the corresponding nanotubes, we shall not hesitate in presenting the simplest possible approaches to electronic structure of the π-electrons when these highlight the importance of topology and connectivity. However, it will also prove useful in the course of the discussion, to refer briefly to calculations of Hartree−Fock quality that have been carried out on a variety of *B* and *C* cages.[3,4]

The outline of the present study is then as follows. Section II below exposes, essentially via Euler's theorem, a one-to-one correspondence between the connectivity of *C* and *B* cages. For example, C_{60} naturally leads to a B_{32} cage. Considerable similarities between the electronic level spectra of both systems are reported. Also briefly discussed is the matter of pentagonal "defects" and the approximate relation to curvature of originally planar graphitic fragments. This is illustrated by a reference to the recent Hartree−Fock calculations on *B* cages of intermediate size already mentioned.

This discussion, involving planar fragments, leads into section III which presents a study of the structure and the electronic properties of boron nanotubes obtained by folding planar sheets of boron atoms. We utilize a (quantum) model akin to Kirchoff's laws of electrical circuits, where evidently connectivity is again an essential ingredient, π-electrons being constrained to move along bonds (wires) joining neighboring nuclei. The dispersion relation of the π-bands is then utilized to calculate (a) constant energy surfaces and (b) the electronic DOS for this two-dimensional (2D) model boron lattice. This latter quantity is compared and contrasted with the study of graphene made in the early work of Coulson.[5] These dispersion relations are then used to obtain the one-dimensional (1D) energy bands and the electronic DOS of boron nanotubes within the "zone folding scheme".[2]

In section IV the theory of the inhomogeneous electron gas[6] is applied self-consistently to infinite nanotubes but now in a surface charge model generalizing the "spherical March model" of C_{60},[7−9] originally designed to deal with tetrahedral (e.g. SiH_4 and GeH_4) and octahedral molecules.[10] It is noteworthy in the present context that central to the March model is the (obviously approximate) assumption that the π-electrons (one per C atom) in C_{60} are distributed spherically. Naturally this is consistent with the uniform surface charge model. However, with this assumption, if we assume the nuclei are constrained on the surface of a sphere, the lowest energy isomer structure will be determined by minimizing the Coulomb repulsion energy between the nuclei. This is a very old problem going back as far as J. J. Thomson. The history is briefly recorded by Berezin[11] together with other possible references. For general *N* point

* Corresponding author e-mail: amovilli@dcci.unipi.it.
[†] University of Antwerp.
[‡] Università di Pisa.
[§] Oxford University.

10.1021/ci0200624 CCC: $27.50
Published on Web 12/03/2003

charges the problem remains mathematically unsolved except for small N. In particular exact solutions are known for $N =$ 4, 6, and 12, and are respectively tetrahedron, octahedron, and icosahedron. For C_{60} a Monte Carlo program written specifically for boron cages[3] demonstrated to numerical accuracy that the European football was extremely close to (if not lowest) the favored isomer for this molecule, provided nuclei are constrained on the surface of the sphere.

The above discussions are then generalized in section V to treat heteronanostructures, earlier work on BN cages[12] being briefly summarized, followed by a reference to fluorinated buckminsterfullerene.[13] The essential new feature in both examples is the electronegativity difference between the component atoms. Section VI constitutes a summary, with some proposals for future directions; the salient one being the use of the progress on quantum current network models (see especially the study of Ringwood[14]) to investigate further topologically disordered networks, which began with the work of Dancz et al.[15]

II. CURVATURE OF GRAPHITIC FRAGMENT, PENTAGONAL DEFECTS, AND A ONE-TO-ONE CORRESPONDENCE BETWEEN CONNECTIVITY OF *B* AND *C* CAGES

A. Use of Euler's Theorem. Amovilli and March[3] performed Hartree−Fock calculations on B_n cages, with n varying from 30 to 54, under the constraint that all B nuclei lie on the surface of a sphere. In correspondence with the "aufbau principle" all boron atoms were found to be either 5- or 6-fold coordinated. They noted that as the number of boron atoms gets large, the number of triangular faces becomes dominant compared to other types of faces in the optimized geometry and the number of pentacoordinated atoms approaches ∼12 for the largest cages, though considerable scatter around this result was found.

In fact, if one assumes *all* faces to be triangular, one can rigorously show that the number of pentacoordinated atoms is *exactly* 12, as we demonstrate immediately below. If all boron faces are triangular, then we have the following relation between the number of boron faces f_B and the number of boron edges e_B

$$e_B = \frac{3}{2} f_B \tag{1}$$

Following the aufbau principle we only have 5- and 6-fold coordinated boron atoms, and so if n_5 and n_6 denote the number of 5- and 6-fold coordinated boron atoms, respectively, then we have that

$$e_B = \frac{5}{2} n_5 + \frac{6}{2} n_6 \tag{2}$$

with the total number of boron atoms n evidently given by

$$n = n_5 + n_6 \tag{3}$$

But now for any closed geometrical figure, the number of faces f, the number of edges e, and the number of vertices v are related through Euler's theorem

$$f + v = e + 2$$

and combining this theorem, where obviously the number of boron vertices $v_B = n$, with eqs 1, 2, and 3 we immediately obtain that $n_5 = 12$ i.e., the number of 5-fold coordinated atoms in boron clusters is uniquely predicted to be 12 if one assumes all faces to be triangular.

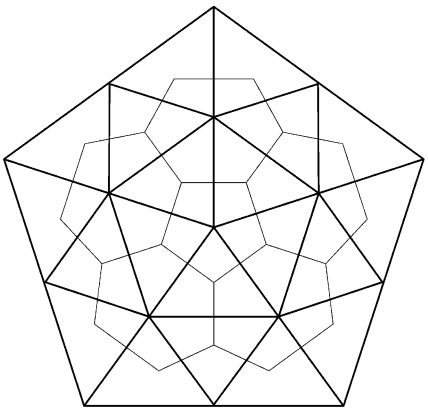

Figure 1. Unfolded section of a hypothetical C_N carbon cage (thin lines) with the corresponding B_n boron cage on top of it (thick lines). Boron cage is constructed by imposing the constraint that every B−B bond crosses exactly one C−C bond. The number of boron atoms is then given by $n = N/2 + 2$.

This is reminiscent of the situation for carbon fullerenes where, as was already noted by Euler, to form a closed figure with hexagons, one always needs exactly 12 pentagons. This similarity inspired us to examine whether a correspondence (or map) between the structure of a B_n boron cage, containing only triangular faces, and the structure of a C_N fullerene, containing only pentagons and hexagons, can be established.

As will be demonstrated below, the only constraint one needs to impose is that every B−B bond crosses exactly one C−C bond. Evidently this implies that there is only one carbon atom in every boron face and vice versa.

First of all, since every carbon atom in a C_N cage is 3-fold coordinated through sp^2 hybridization, the crossing of the bonds is a sufficient condition to ensure that all boron faces are triangular as is required. Second, as is clear from Figure 1, a pentagonal "defect" in a C_N cage (a pentagon surrounded by five hexagons, see Figure 1, the thin lines) will generate a corresponding pentagonal defect in a boron cage (a pentacoordinated atom surrounded by five hexacoordinated atoms, see Figure 1, the thick lines). On the other hand, as one can easily check, sections of the C_N cage containing only hexagons will generate only 6-fold coordinated boron atoms.

So a natural correspondence between the structure and connectivity of C_N carbon cages and that of B_n boron cages (with only triangular faces) is exposed. To find out precisely which B_n boron cage we obtain in this way starting from a certain C_N cage we again turn to Euler's theorem. Starting from a carbon cage C_N, we have obviously N vertices, and hence

$$f_c = e_c + 2 - N \tag{4}$$

With constant 3-fold coordination, it follows that the number of edges, e_c, is equal to 3/2 N and hence, inserting this value into eq 4 one reaches the result for C_N cages that

$$f_c = \frac{N}{2} + 2 \tag{5}$$

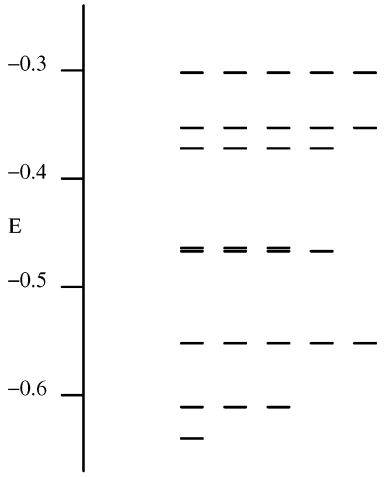

Figure 2. Hartree−Fock values of the π-electron level spectrum of C_{60}. The degeneracies are in good agreement with predictions from Hückel theory.

Since our construction implies one boron atom in every carbon face, the number of carbon faces f_c obviously equals the number of boron vertices v_B (=n), and we obtain the following one-to-one relation between N and n.

$$n = \frac{N}{2} + 2 \qquad (6)$$

Equation 6 applied to buckminsterfullerene itself with N = 60 yields n = 32, i.e., the cage B_{32} is its analogue. Note that this correspondence is purely topological. Whether or not realistic values for the bond lengths in C_N carbon cages and B_n boron cages allow for the mapping we propose in Figure 1 is not relevant. Since the faces in B_n boron cages become predominantly triangular only in the limit of large n, we expect the correspondence to become especially relevant for large B_n boron clusters.

B. Electronic Structure of π-Electrons in C_{60} and Valence Electrons in B_{32}. Having emphasized topology and connectivity above, let us first record the one-electron eigenvalues obtained by Amovilli et al.[4] from Hartree−Fock calculations for C_{60}. To emphasize the degeneracies plus near degeneracies, the reader may refer to Figure 2. As is readily verified, filling these depicted π-eigenvalues with two electrons per level shows that the upper state is the HOMO level.

Turning to B_{32}, a large number of eigenvalues for the valence orbitals were obtained in the Hartree−Fock study of Amovilli and March.[3] Their degeneracies (or near degeneracies) are depicted in Figure 3. Filling the lowest four graphs of levels would deal with B_{32} itself if one assumes one π-electron per atom, which is a chemical oversimplification however.

C. Pentagonal Defects and Curvature. To complete the present section, we wish to add some comments on cage curvature in relation to pentagonal defects (see also ref 4). If we discuss fullerenes in particular, we first note that there will be appreciable anisotropic curvature at the equilibrium geometries. To illustrate this, a best candidate for uniform curvature is a fullerene with the pentagonal defects spread as uniformly as is feasible: i.e., to form an icosahedral-

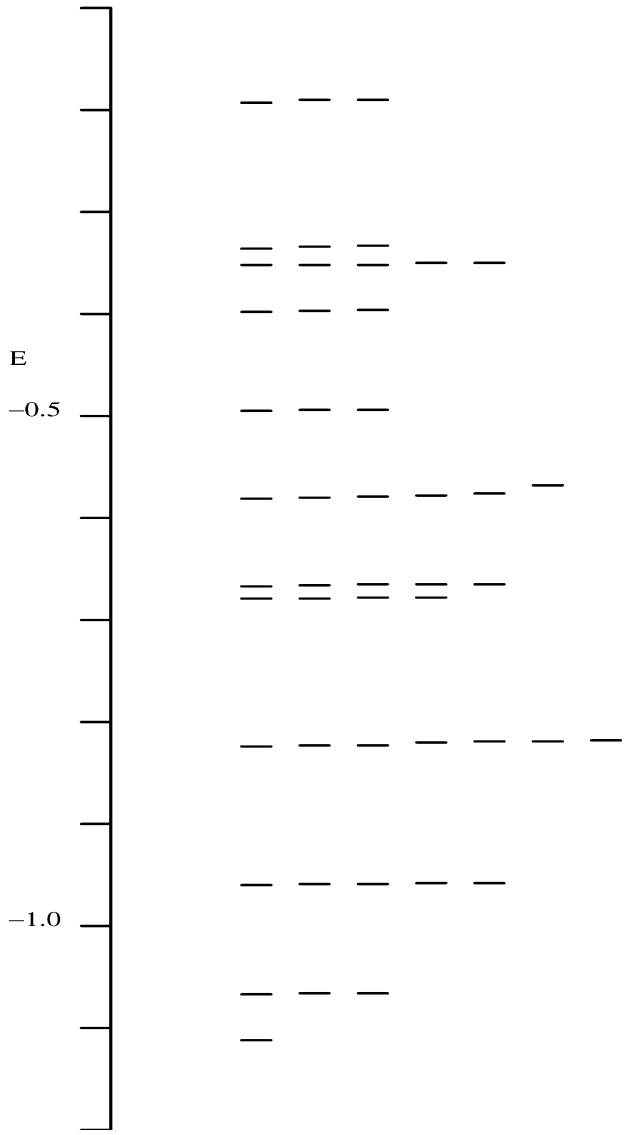

Figure 3. Hartree−Fock values for the valence electron level spectrum of B_{32}.

symmetry cage. For such a fullerene (which we conceive for the C_N cage in the large N limit) the pentagons can be visualized to reside at the corners of an icosahedron-type superstructure, all the remaining rings being hexagons. Then it is helpful to consider a graphitic region corresponding to a triangular face of the above superstructure, all the remaining rings being hexagons. The area of this face as measured on the surface of a uniformly curved spherical surface of radius R is evidently $A_{curved} = (4\pi R^2)/20$, there being 20 such faces. The length l of the side of such a "spherical triangle" is θR; here θ denotes the angle subtended by the edge as viewed from the center of the sphere. The area of a planar triangle with edges of the same length is $A_{plane} = \sqrt{3}/4l^2$. But A_{plane} (corresponding to an unstrained part of graphene) is different, of course, from A_{curved}, and there is a strain σ per C atom given by[4]

$$\sigma \sim \{A_{plane}/(N/20)\}^{1/2} - \{A_{curved}/(N/20)\}^{1/2} \qquad (7)$$

such a strain occurring for each bond in the graphitic portion

of the network. Therefore, with $\sim 3N/2$ such bonds, the total stress is

$$E_{\text{stress}} \approx (3N/2)\frac{1}{2}k\sigma^2 \tag{8}$$

where k denotes a suitable force constant appropriate for C−C aromatic bonds. Substituting eq 7 into eq 8 it follows that

$$E_{\text{stress}} \sim 15k\left(\frac{3^{1/4}}{2}\theta - \left\{\frac{\pi}{5}\right\}^{1/2}\right)^2 R^2 \tag{9}$$

But the equilibrium R is determined well by the "rule" of constant surface area per atom[3,4] i.e. $R^2 \sim N$ and so from eq 9 stress is important. If some structure other than that of icosahedral symmetry is assumed for the arrangement of the pentagons, the geometric factor in eq 9 will be modified but will remain nonzero.

The question as to the relief of such curvature strain then arises (still one is considering the large N limit). Once more, as a prototypical example, the arrangement of icosahedral symmetry can be taken. One then visualizes the structure to deform to resemble a icosahedron superstructure, having the pentagon at its apexes. Then the triangular graphitic regions already discussed can be viewed as changed from their spherically curved forms to almost planar regions with anisotropic curvature at the edges which connect each triangular region to adjacent ones. Within the planar triangular areas there is neither strain nor stress: instead it occurs at the edges of the triangles. The total amount of such an edge is $\sim 30R \propto N^{1/2}$, so that the stress is reduced to $E'_{\text{stress}} \propto N^{1/2}$. The proportionality constant can again be expected to depend on the way the pentagons are dispersed, the overall conclusion being that geometric Gaussian curvature is preferably localized in the region of the pentagons, with then some anisotropic curvature (without Gaussian curvature) mediating between such adjacent parts, as noted in ref 4. Computations on large nonopen-shell icosahedral-symmetry fullerenes reveal the proposed polyhedralization in diagrams of the geometry optimized structures (most clearly for C_{240}; the largest treated).

In C nanotubes one can intuitively measure the stress as the deviation from linearity of three adjacent atoms lying on a circle of a section of the nanotube. The angle measuring this deviation is proportional to $1/n$ where n is the number of C atoms on this circular section. The stress energy per atom is thus proportional to $1/n^2$, and the total stress energy per unit length is proportional to $1/n$ which behaves as $1/R$, R being the radius of the tube.

Having referred in some detail above to the graphitic layers, we follow this account by taking a planar "model boron" structure and using again topology and connectivity to discuss the π-electronic energy band structure. As was reported in the paper by Boustani et al.[16] preliminary experimental results for pure-boron systems seem to confirm the existence of boron sheets. We will consider here a purely planar boron configuration and apply the simplest possible theories to extract the main features of the DOS which arise from topological aspects.

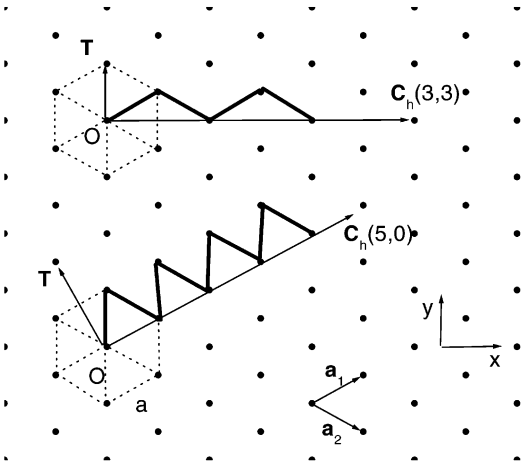

Figure 4. Model boron lattice. Translational vector **T** and chiral vector $\mathbf{C}_h$ defining the unit cell of the nanotube are shown. Special choices for the chiral vector $\mathbf{C}_h(n, n)$ and $\mathbf{C}_h(n, 0)$ are shown to lead to isosceles zigzag symmetry and equilateral zigzag symmetry, respectively.

III. ELECTRONIC PROPERTIES OF BORON NANOTUBES

A. Structure of a Single Wall Boron Nanotube. *1. Equilateral and Isosceles Zigzag Symmetry.* We start by describing the model planar boron lattice which will then be folded to obtain boron nanotubes. The structure of the boron lattice we consider can be obtained simply by considering an ordinary sheet of graphene in which we replace all carbon atoms by boron atoms and place an additional boron atom in the center of every hexagon. In this way, every boron atom has a near-neighbor coordination, say c, equal to 6. The resulting lattice is shown in Figure 4.

To describe this lattice one can use two lattice vectors, say $\mathbf{a}_1$ and $\mathbf{a}_2$, which are either 120° apart, or 60° apart. If one only wants to describe the 2D lattice, both choices are of course equivalent. However, if one wants to use these lattice vectors to describe the nanotubes obtained by folding the 2D sheet, then the choice where both lattice vectors are 60° apart is the most convenient as became apparent for carbon nanotubes.

To describe a nanotube obtained by folding a sheet, one starts by defining the so-called chiral vector $\mathbf{C}_h$.

$$\mathbf{C}_h = n\mathbf{a}_1 + m\mathbf{a}_2 \tag{10}$$

This vector connects by definition two lattice points on the sheet which have to be connected when one folds the sheet into a tube and the specific choice for n and m completely determines the structure of the resulting tube. From the definition of the chiral vector $\mathbf{C}_h$ it is clear that its length equals the circumference L of the resulting nanotube which is then given by

$$L = a\sqrt{n^2 + m^2 + nm} \tag{11}$$

with $a = |\mathbf{a}_1| = |\mathbf{a}_2|$.

Similar to carbon, all possible distinct seamless nanotubes can be obtained by choosing a set of indices (n, m) with n any integer number and m ranging from 0 to n. However, an interesting feature then arises when one is dealing with boron. As one can easily see in Figure 4 both the nanotube

generated by a $\mathbf{C}_h(n, n)$ chiral vector and that generated by the $\mathbf{C}_h(n, 0)$ vector now have in essence zigzag symmetry. However, as is clear from Figure 4 in the case $n = m$ we have *isosceles triangles* (two equal sides), while in the case $m = 0$ we have *equilateral triangles* (three sides equal) triangles. For simplicity we will refer to these limiting cases as (n, n) i-*zigzag* and $(n, 0)$ e-*zigzag* symmetry respectively where "i" then evidently stands for isosceles and "e" for equilateral.

We will now go on to define the unit cell of our boron nanotube and the corresponding Brillouin zone. Except for a few details this is identical to the carbon case, and we refer the reader to the excellent book by Saito, Dresselhaus, and Dresselhaus[2] for more details.

The vector perpendicular to $\mathbf{C}_h$ going from the chosen origin to the nearest lattice point defines the translational vector of our 1D periodic nanotube and is given by

$$\mathbf{T} = t_1\mathbf{a}_1 + t_2\mathbf{a}_2$$

with the relation between t_1, t_2, and m, n unchanged as compared to the carbon system namely

$$t_1 = \frac{2m + n}{d_R}, \quad t_2 = -\frac{2n + m}{d_R} \tag{12}$$

where d_R is the greatest common divisor (gcd) of $(2m + n)$ and $(2n + m)$. The rectangle generated by these two vectors $\mathbf{C}_h$ and $\mathbf{T}$ is the unit cell of our boron nanotube, where the translational vector $\mathbf{T}$ determines the direction in which the unit cell repeats itself periodically.

2. Reciprocal Space. The reciprocal space of the boron sheet is generated by the reciprocal lattice vectors $\mathbf{b}_1$ and $\mathbf{b}_2$ defined by

$$\mathbf{b}_i.\mathbf{a}_j = 2\pi\delta_{ij}$$

We define the vectors in the reciprocal space of the nanotube by the relations

$$\mathbf{C}_h.\mathbf{K}_1 = 2\pi \quad \mathbf{T}.\mathbf{K}_1 = 0 \tag{13}$$

$$\mathbf{C}_h.\mathbf{K}_2 = 0 \quad \mathbf{T}.\mathbf{K}_2 = 2\pi \tag{14}$$

which then immediately leads to the result

$$\mathbf{K}_1 = \frac{1}{N}(-t_2\mathbf{b}_1 + t_1\mathbf{b}_2) \quad \mathbf{K}_2 = \frac{1}{N}(m\mathbf{b}_1 - n\mathbf{b}_2) \tag{15}$$

with

$$N = mt_1 - nt_2 = \frac{|\mathbf{C}_h \times \mathbf{T}|}{|\mathbf{a}_1 \times \mathbf{a}_2|} = \frac{2(m^2 + n^2 + nm)}{d_R} \tag{16}$$

with $\mathbf{b}_1$ and $\mathbf{b}_2$ the lattice vectors of the graphene Brillouin zone and N the number of atoms in the unit cell of the nanotube. Note that for the carbon sheet the number of carbon atoms in the nanotube unit cell was given by $2N$.

Since the boron lattice we consider can be obtained from taking only the *lattice* points in a graphene layer (points with identical physical environment), the Brillouin zone of the boron and the carbon sheet have identical symmetries.

3. Energy Bands within the Zone Folding Scheme. Within the zone folding scheme[2] one essentially assumes that the motion of the electrons in a real single wall 3D nanotube can be described by the motion of the electrons in the planar 2D strip from which that specific nanotube can be obtained by folding. To obtain the energy dispersion relations for the boron nanotube we first need to determine the energy dispersion relation of the boron sheet, say $E_{2DB}(\mathbf{k})$, for all possible $\mathbf{k}$-values and then restrict ourselves only to those $\mathbf{k}$-values which are consistent with the boundary conditions for motion of the electrons on the strip which generates the boron nanotube.

Since the unit cell of the nanotube (or the infinitely long strip) defined by $\mathbf{T}$ and $\mathbf{C}_h$ repeats itself periodically only in one dimension (in the direction of $\mathbf{T}$), the motion of the electrons along that direction is characterized in $\mathbf{k}$-space by a quasi-continuous scalar wave-vector k in a one-dimensional Brillouin zone of length $2\pi/T$ in the direction of $\boldsymbol{K}_2$. The boundary conditions along the direction of the chiral vector $\mathbf{C}_h$ yield a discrete number (equal to N) of allowed values for the component of the wave-vector in the direction of $\boldsymbol{K}_1$ given by $\mu(2\pi/|\mathbf{C}_h|)$ (or equivalently $\mu|\boldsymbol{K}_1|$) with $\mu = 0, ..., N - 1$.

Combining this we find that the allowed $\mathbf{k}$-values lie on a set of N parallel lines in $\mathbf{k}$-space directed along $\boldsymbol{K}_2$ and separated by $\boldsymbol{K}_1$. Every line represents the 1D Brillouin zone but for a different value of the component of the wave-vector along $\boldsymbol{K}_1$. The energy values for these wave-vectors are obtained by taking cross sections along these lines of the energy surface of the full 2D boron sheet. Every cross-section then gives a band in the 1D Brillouin zone of the nanotube.

We then find for the energy dispersion relations for a single wall nanotube within the zone folding scheme[2]

$$E_\mu(k) = E_{2DB}\left(k\frac{\mathbf{K}_2}{|\mathbf{K}_2|} + \mu\mathbf{K}_1\right)\left(-\frac{\pi}{T} < k < \frac{\pi}{T}\right) \tag{17}$$

with the band index μ given by

$$\mu = 0, ..., N - 1 \tag{18}$$

and with $T = |\mathbf{T}|$. We now first turn to the determination of the energy dispersion relation $E_{2DB}(\mathbf{k})$ for the planar boron sheet.

B. Electronic Structure of the 2D Boron Sheet. *1. 2D Energy Dispersion Bands.* For the energy band of the 2D boron sheet we obtain within the Quantum Network (QN) (see Appendix A) model the relation

$$E_{2DB}^{QN}(\mathbf{k}) = \frac{q^2}{2} = \frac{1}{2}\left\{\frac{1}{a}\cos^{-1}\left(\frac{1}{c}S(\mathbf{k})\right)\right\}^2 \tag{19}$$

The structure factor $S(\mathbf{k})$ appearing in eq 19 is defined by

$$S(\mathbf{k}) = \sum_{j=1}^{c} e^{i\mathbf{k}.\mathbf{a}_j} \tag{20}$$

where the vectors $\mathbf{a}_j$ connect every lattice position $\mathbf{R}$ to its c nearest neighbors. On the other hand, from the tight binding (TB) method we obtain the relation (see Appendix B)

$$E_{2DB}^{TB}(\mathbf{k}) = \epsilon_\pi + tS(\mathbf{k}) \tag{21}$$

with ϵ_π and t defined in Appendix B. Since we are mainly interested in qualitative electronic properties which arise as

a consequence of the periodicity and topology of the system under consideration, we have assumed in our tight binding calculations the following simple values (assumed arbitrarily in atomic units) for the parameters.

$$\epsilon_\pi = 0,\ t = -1 \text{ (au)} \tag{22}$$

The important point to stress here is that both expressions for the energy depend on the wave-vector **k** through the same structure factor $S(\mathbf{k})$ for which we will derive an explicit expression immediately below.

Note that the wires in B networks cannot be seen as two-electron bonds as in C networks. Let us take for example the B_7H_6 molecule in a D_{6h} (planar hexagonal) geometry, similar to that of benzene but with an extra B atom on the symmetry center. In this molecule the central atom, apparently hexacoordinated, participates to the stabilization by accommodating its three valence electrons in the lowest energy π orbitals, otherwise completely empty. Although in this case a Jahn−Teller distortion is expected, at the equilibrium geometry the B_7H_6 electron structure is dominated by the above situation. In larger quasi-planar B clusters the σ electron distribution tends to be the result of a resonance of graphitic-like structures which leave in turn B atoms bonded only through delocalized π orbitals. In our B planar lattice each atom provides two valence electrons to the σ distribution and one valence electron to the π distribution. A population analysis performed on quasi planar B lattices has been performed by Boustani,[17] and his results support the above picture.

2. Expression for the Structure Factor S(k) within a Given Reference Frame. In particular we start by choosing the $x - y$ coordinate system in the same direction relative to the lattice vectors $\mathbf{a}_1$ and $\mathbf{a}_2$ as in Figure 4. This then yields for the coordinates of both lattice vectors

$$\mathbf{a}_1 = \left(\frac{\sqrt{3}}{2}a, \frac{a}{2}\right), \quad \mathbf{a}_2 = \left(\frac{\sqrt{3}}{2}a, -\frac{a}{2}\right) \tag{23}$$

where the lattice constant a is now equal to the B−B bond length a_{B-B}. (Note that for graphene we have the relation $a = \sqrt{3}a_{C-C}$). We choose $\mathbf{a}_3$ along the positive y-axis which yields for the coordinates

$$\mathbf{a}_3 = (0, a) \tag{24}$$

All near neighbor points can then be reached by the vectors $\pm\mathbf{a}_i$ ($i = 1...3$). We can then further evaluate the expression for the structure factor to obtain

$$S(\mathbf{k}) = \sum_{j=1}^{c} e^{i\mathbf{k}.(\mathbf{a}_j)}$$

$$= 2\sum_{j=1}^{3}\cos(\mathbf{k}.\mathbf{a}_j)$$

$$= 2\cos(ak_y) + 4\cos\left(\frac{\sqrt{3}}{2}ak_x\right)\cos\left(\frac{1}{2}ak_y\right) \tag{25}$$

As mentioned above, this structure factor is common to both the QN model and the tight binding result.

3. Constant Energy Surfaces and DOS of the 2D Boron Sheet. The constant energy contours from the QN model are given in Figure 5. Similar to the carbon case, we note that also here so-called "trigonal warping effect"[18] occurs, whereby the constant energy contours change from the circular behavior around the center and the *K*-points to a triangular shape near the *M* points.

The DOS_{2D} of the 2D energy bands can then be calculated from the expression

$$DOS_{2D}(E) = \frac{2}{(2\pi)^2}\int \frac{ds}{|\nabla_{\mathbf{k}}E(\mathbf{k})|} \tag{26}$$

where the line integral is along a surface of constant energy E. Returning to the constant energy surfaces in Figure 5, we have performed the line integration in eq 26 with $E(k)$ given for the "model boron lattice" by eq 19 with $c = 6$, and the results are depicted in Figure 6. It is worthwhile to compare and contrast the form of $N(E)$ shown here with the π-bands for graphite first obtained by Coulson[5] using the same QN model. First, the π-bands touched in graphite, at the point where $N(E) = 0$, i.e., one had semimetallic behavior (both zero gap and zero $N(E_F)$) at the Fermi (or HOMO) level E_F. In contrast, the model boron lattice, by counting the π-electrons, is metallic (zero gap and nonzero $N(E_F)$ at the *HOMO* level). A van Hove singularity (vHs) arises near the edge of the Brillouin zone where the energy bands level off due to periodicity. Results from the tight binding method yielded similar results for all features.

C. 1D Energy Bands of (*n, n*) i-Zigzag Boron Nanotubes. Within the chosen orientation for the $x - y$ coordinate system, the chiral vector $\mathbf{C}_h$ (and correspondingly also $\boldsymbol{K}_1$) is directed along the positive x-axis for the special case where $m = n$. Whereas for graphene this special choice for the indices leads to nanotubes exhibiting armchair symmetry, in the case of boron it leads to *i*-zigzag symmetry, as discussed above. Applying periodic boundary conditions along the circumferential direction then leads to the quantization

$$k_{x,j} = \frac{2\pi}{n\sqrt{3}a}j \qquad (j = 1, ..., 2n) \tag{27}$$

This then yields for the *i*-zigzag structure factor $S_j^{iz}(\mathbf{k})$

$$S_j^{iz}(k) = 2\cos(ak) + 4\cos\left(\frac{\pi j}{n}\right)\cos\left(\frac{ak}{2}\right) \tag{28}$$

$$(j = 1, ..., 2n) \qquad \left(-\frac{\pi}{a} < k < \frac{\pi}{a}\right)$$

where j now denotes the band index. From this expression, one can immediately write down the corresponding expression for the (n, n) energy bands $E_j^{iz}(k)$, either in the tight binding approximation or from the Quantum Network model.

Figure 7 (a) shows the energy bands obtained from the QN method for a boron (3, 3) *i*-zigzag nanotube which has from eq 11 a circumference $L \approx 5.20a$. Clearly since $\boldsymbol{K}_1$ is directed along a symmetry axes of the 2D Brillouin zone, we have energy bands symmetrical around the origin. From tight binding calculations we found a similar set of bands, with the same general form and degeneracy.

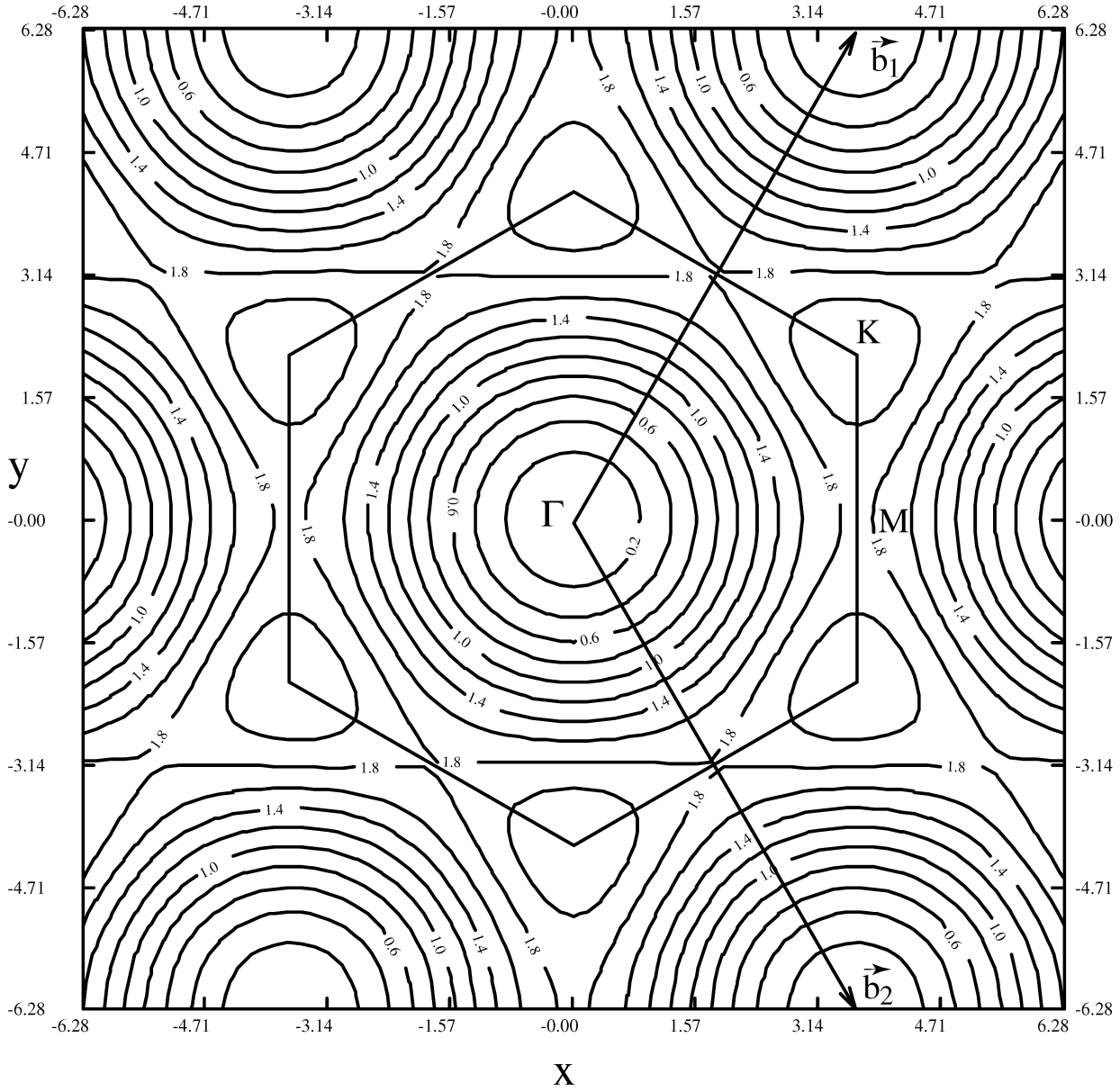

Figure 5. Brillouin zone of the boron lattice. Constant energy contours (with values in atomic units) for the quantum network model are shown. Trigonal warping effect causes deviation from spherical behavior near the center and *K* points toward triangular behavior near the *M* points.

D. 1D Energy Bands of (*n*, 0) e-Zigzag Boron Nanotubes. We will now go on to derive an expression for the energy bands in the special case that $m = 0$. As in the case of graphene this leads to zigzag nanotubes but as discussed above, we now need to make the extra specification that we are dealing with equilateral zigzag symmetry. To obtain an explicit expression for the energy bands it is helpful to consider a coordinate transformation to a more suitable reference system. Following Saito, Dresselhaus, and Dresselhaus[2] we consider a passive coordinate transformation counterclockwise over 120°. This implies we now use the $x - y$ coordinate system depicted in their Figure 4.3(b). This transformation leaves the expression for the structure factor (25) unchanged as one can easily check but brings the chiral vector $\mathbf{C}_h$ for the (n, 0) system under consideration along the (negative) y-axis. Again applying periodic boundary conditions along the circumferential direction leads to the quantization

$$k_{y,j} = \frac{2\pi}{na} j \qquad (j = 1, ..., 2n) \tag{29}$$

For the *e*-zigzag structure factor $S_j^{ez}(k)$ one then obtains

$$S_j^{ez}(k) = 2\cos\left(\frac{2\pi}{n} j\right) + 4\cos\left(\frac{\pi j}{n}\right)\cos\left(\frac{\sqrt{3}}{2} ak\right) \tag{30}$$

$$(j = 1, ..., 2n) \qquad \left(-\frac{\pi}{\sqrt{3}a} < k < \frac{\pi}{\sqrt{3}a}\right)$$

from which one can again immediately obtain the corresponding (n, 0) energy bands $E_j^{ez}(k)$, with j again denoting the band index. The resulting energy bands from the QN model are plotted in Figure 7(b). We chose a value for n

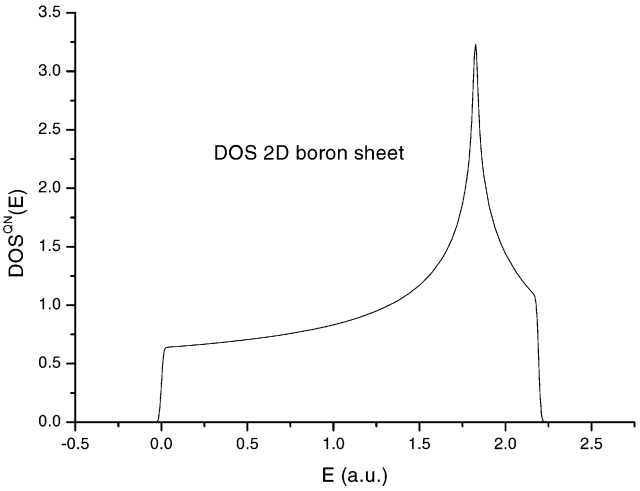

Figure 6. Density of states (including spin degeneracy) for the 2D boron sheet. Outstanding feature is the van Hove singularity near the edge of the first Brillouin zone.

which yields approximately a nanotube of the same radius as for the (3, 3) zigzag tube, namely $n = 5$ which yields for the circumference $L = 5a$.

E. 1D Energy Bands for General Chiral Symmetry. For a general (*n*, *m*) system we go back to the original coordinate system (as for the armchair nanotubes). The coordinates of the lattice vectors $\mathbf{b}_1$ and $\mathbf{b}_2$ in reciprocal space are then given by

$$\mathbf{b}_1 = \left(\frac{2\pi}{\sqrt{3}a}, \frac{2\pi}{a}\right), \mathbf{b}_2 = \left(\frac{2\pi}{\sqrt{3}a}, -\frac{2\pi}{a}\right) \qquad (31)$$

which implies the relations

$$\mathbf{b}_1.\mathbf{b}_1 = \mathbf{b}_2.\mathbf{b}_2 = \frac{4}{3}\left(\frac{2\pi}{a}\right)^2 \text{ and } \mathbf{b}_1.\mathbf{b}_2 = -\frac{2}{3}\left(\frac{2\pi}{a}\right)^2 \qquad (32)$$

We then obtain for the *x* and *y* components of the vector $k\boldsymbol{K}_2/|\boldsymbol{K}_2| + \mu\boldsymbol{K}_1$

$$k_x = \frac{k}{|\mathbf{K}_2|}\left[\frac{m-n}{N}\right]\left(\frac{2\pi}{\sqrt{3}a}\right) + \mu\left[\frac{m+n}{N}\right]\left(\frac{2\pi}{a}\right)\sqrt{3} \qquad (33)$$

$$k_y = \frac{k}{|\mathbf{K}_2|}\left[\frac{m+n}{N}\right]\left(\frac{2\pi}{a}\right) + \mu\left[\frac{n-m}{N}\right]\left(\frac{2\pi}{\sqrt{3}a}\right) \qquad (34)$$

with

$$|\mathbf{K}_2| = \sqrt{\mathbf{K}_2.\mathbf{K}_2} = \sqrt{\left[\left(\frac{m}{N}\right)^2 + \left(\frac{n}{N}\right)^2\right]\mathbf{b}_1.\mathbf{b}_1 - 2\left(\frac{nm}{N}\right)\mathbf{b}_1.\mathbf{b}_2} \qquad (35)$$

and the dependence of *N* on *m* and *n* given by eq 16. For a general choice of *n* and *m*, the number of atoms in the unit cell of the nanotube and correspondingly the number of 1D dispersion relations gets very large compared to the simpler (*n*, *n*) and (*n*, 0) cases and is less insightful.

F. Density of States of One-Dimensional Boron Nanotubes. We now calculate the DOS per boron atom from these 1D energy dispersion relations using the formula

$$\mathrm{DOS}(E) = \frac{2}{(2\pi)}\frac{|\mathbf{T}|}{N}\sum_{\mu=1}^{N}\int \delta(E - E_\mu(k))dk \qquad (36)$$

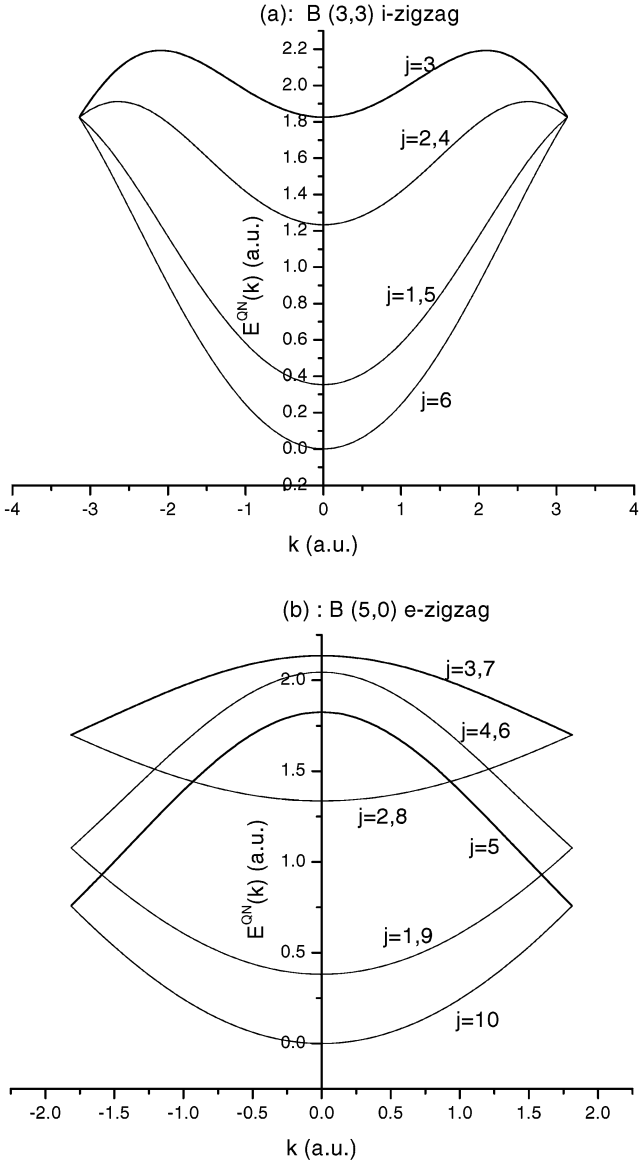

Figure 7. (a): 1D energy dispersion relations from the QN model for a boron (3, 3) *i*-zigzag nanotube. The band index is denoted by j. (b): 1D energy dispersion relations from the QN model for a boron (5, 0) *e*-zigzag nanotube.

where the integration is over the 1D Brillouin zone of the nanotube, and the summation is over all bands denoted by the index μ. The results are shown in Figure 8(a),(b) for the (3, 3) *i*-zigzag tube and the (5, 0) *e*-zigzag tube, respectively. Obviously since the first cuts in the 2D energy bands of the boron sheet are within the region where the constant energy contours are circular, irrespective of the direction of $\mathbf{C}_h(n, m)$ we find a similar DOS for the low energy values. On the whole we find that the DOS looks similar, the main difference being that the two peaks which were nearly degenerate for the (3, 3) *i*-zigzag tube are further apart for the (5, 0) *e*-zigzag tube.

All of the boron nanotubes we considered were found to be metallic. Of course, we must expect also here that a Peierls distortion[2] will occur which will then possibly open a small gap in the DOS of the first energy band, but this is beyond the scope of the present study.

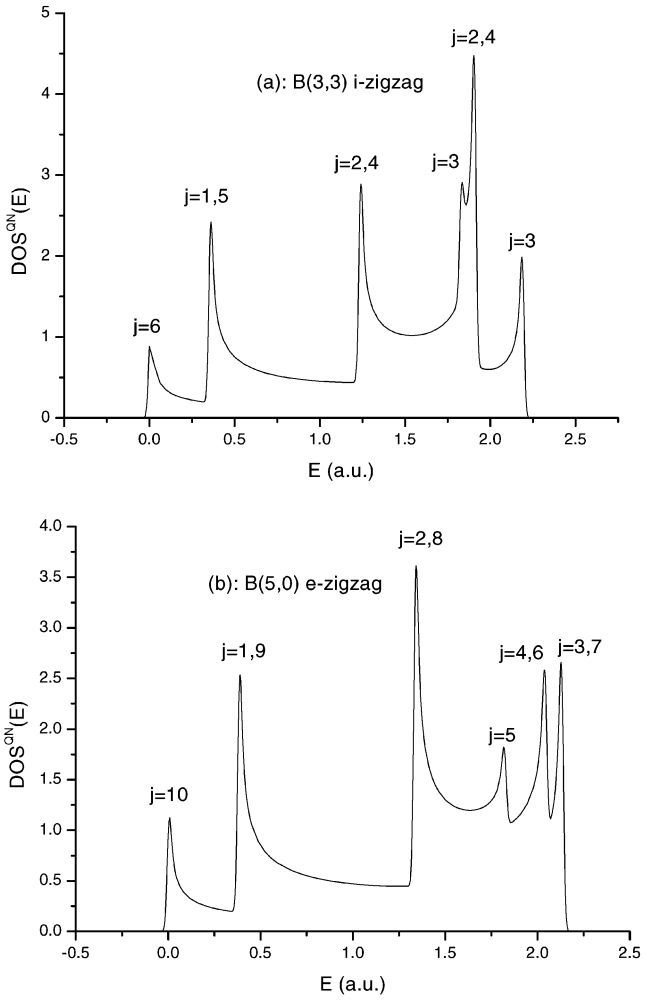

Figure 8. (a): DOS from the QN model for a boron (3, 3) *i*-zigzag nanotube. (b): DOS from the QN model for a boron (5, 0) *e*-zigzag nanotube.

IV. "THE MARCH MODEL" APPLIED TO NANOTUBES

Contrary to the density of states, we expect other quantities relating to the electrons to be only very slightly dependent on the detailed structure of the carbon or boron frame. To exemplify this point Leys et al.[19] calculated the self-consistent field in which the 2s and 2p valence electrons move in an isolated carbon nanotube under the assumption that the positive charge of the C^{4+} ions can be smeared out *uniformly* over the surface of an infinitely long cylinder, thereby neglecting all structure and only retaining the basic cylindrical symmetry of the problem. The spirit of this assumption goes back to the early work of March[10] on tetrahedral and octahedral molecules where, for instance in GeH_4, the external field in which the electrons move was approximated by smearing out the four H protons over the surface of a sphere of equal radius to the Ge−H bond length and centered on the Ge nucleus. The inhomogeneous electron gas created by this model external potential was then treated using the Thomas-Fermi method. In evaluating the nuclear−nuclear potential energy however the correct geometry of the nuclear framework was always retained. This method has recently experienced renewed interest. Thus the work of Clougherty and Zhu[7] on C_{60} calculated the equilibrium cage radius for C_{60} using the method they termed the March model. Further

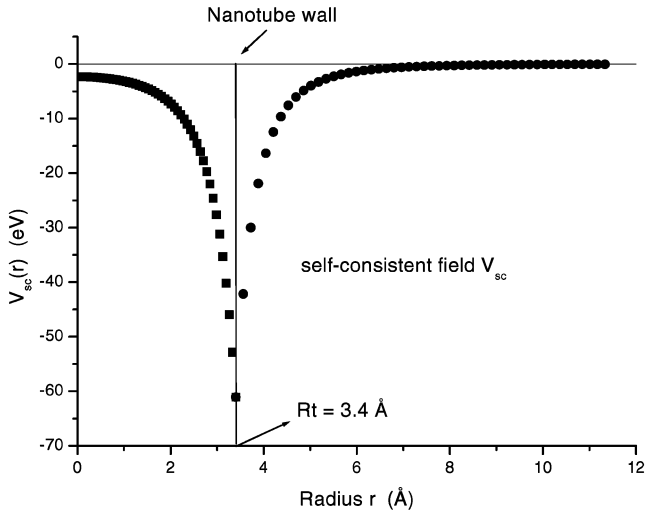

Figure 9. Self-consistent field for an isolated single wall nanotube from the March model. In calculating the surface charge, the C−C bond length was taken to be 2.68 au.

studies include those of Despa,[8] also on C_{60}, and Amovilli and March[3] on boron cages. (See also ref 9.) We will now briefly summarize the main results of the study of Leys et al.[19]

If we take $\Theta(r)$ to be minus the self-consistent potential $V_{sc}(r)$ we obtain for $\Theta(r)$ the differential equation

$$\frac{\partial^2\Theta}{\partial r^2} + \frac{1}{r}\frac{\partial\Theta}{\partial r} = c\Theta^{3/2} \qquad c = \frac{2^{7/2}}{3\pi} \tag{37}$$

where r denotes the distance from the axis of the tube. This equation was solved subject to the appropriate boundary conditions, and in particular the surface charge σ was taken into account through the boundary condition at the radius R_t of the tube

$$\left(\frac{\partial\Theta_1}{\partial r}\right)_{R_t} = 4\pi\sigma + \left(\frac{\partial\Theta_2}{\partial r}\right)_{R_t} \tag{38}$$

where Θ_1 denotes the solution inside the tube and Θ_2 outside the tube. The condition 38 reflects the discontinuity in the electric field across the surface charge.

Figure 9 shows our results for the potential $V_{sc}(r)$. The data used in determining σ is mentioned in the captions. Östling et al.[20] performed full Kohn−Sham calculations on the same model system, and we have used their results for comparison. The electron density $\rho(r)$ was found to be reasonably well described by TF theory, but we especially found very good agreement for the self-consistent potential $\Theta(r)$, both qualitatively and quantitatively. Moreover, in the same study, Östling et al. compared their results with those obtained from tight binding when the exact atomic positions were taken into account and found only very small differences from their Kohn−Sham results on the model system. This clearly indicates that we can expect also our results, following the original procedure of March, to be a good approximation to the self-consistent field. Obviously the main merit of our work is its relative simplicity allowing one to obtain analytic results in certain cases, for instance for the

power law behavior at large r which was found to be

$$\Theta(r) = \left(\frac{16}{c}\right)^2 \frac{1}{r^4}\left[1 + \frac{F_1}{r^c} + \text{higher order terms}\right] \quad \text{with } c = 2\sqrt{6} - 4 \quad (39)$$

and F_1 is an integration constant.

V. HETERONANOSTRUCTURES

So far we have focused our attention on the homonuclear cases of *B* and of *C*. In this penultimate section, we shall extend these considerations to two specific heteronuclear systems: (i) BN cages and (ii) fluorinated buckminsterfullerene. We shall take these in turn below.

A. Boron Nitride Cages: Effect of Electronegativity Difference on Electronic Structure. Let us commence this section on BN with two general references to this area: (a) the work of Niedenzu and Dawson[21] on boron−nitrogen compounds and (b) the more technologically oriented work on the synthesis and properties of boron nitride edited by Pouch and Alterovitz.[22]

With no electronegativity difference included, Figure 6 of ref 12 shows the Hückel π-bands of the structures depicted in Figure 5 of the same reference. It is immediately clear from the uppermost and the lowest parts of their Figure 6 that the π-bands touch, whereas for the other three structures depicted in their Figure 5 there are energy gaps. But when electronegativity is included in the Hückel treatment (i.e. $\alpha_B \neq \alpha_N$), the zero-gap cases with $\alpha_B = \alpha_N$ also have energy gaps: the most important consequence of the electronegativity difference. Zhu et al.[12] also have used the so-called extended Hückel model, but although the bands change somewhat in detailed shape the salient feature of the electronegativity as introducing energy gaps where originally π-bands touched is confirmed.

B. Fluorinated Buckminsterfullerene. A highly fluorinated fullerene, a D_3 isomer of $C_{60}F_{48}$, has recently been investigated by *X*-ray fluorescence spectroscopy.[13] The results of such a study have been interpreted by quantum mechanical calculations. In particular, it has been confirmed that the contribution to the electron density of frontier orbitals, namely the occupied orbitals with the highest energy, comes from six localized CC double bonds. Evidently, the higher electronegativity of fluorine causes, in this case, a localization of the π cloud of fullerene in the C−F bond regions, which are in fact essentially orthogonal to the carbon cage surface. The 12 carbon atoms which are not bonded to fluorine thus determine six isolated CC double bonds. Within a very simple Hückel-like formalism the situation can be simulated by substituting 48 of the 60 p functions of fullerene by the same number of σ C−F bond functions and also by reducing the connectivity, namely the bond order, between all neighbor pair of functions in which one of them is a C−F bond orbital. Furthermore, the energy of C−F bond functions must be shifted to lower energies with respect to the p carbon atomic orbitals. The resulting molecular orbitals are then split essentially in to three bands. The lowest energy band is built from 48 occupied orbitals, which represent the 48C−F σ electron cloud, the intermediate band being constructed from 6 occupied orbitals, representing the 6 isolated π C−C double bonds, and, finally, the highest energy band which includes the 6 empty π CC antibonding orbitals.

VI. SUMMARY AND FUTURE DIRECTIONS

We have stressed the way pentagonal defects, present say in a C_{60} cage, can be connected with the curvature introduced into an originally planar graphitic strip. Using Euler's theorem, a one-to-one correspondence between the geometry of *B* cages and *C* cage structures has been proposed. This has led us to embed topology and connectivity into a quantum current network approach to a model boron two-dimensional lattice. The electronic band dispersion relation $E(\mathbf{k})$ for this lattice has been employed to obtain (i) constant energy E surfaces in the $\mathbf{k} = (k_x, k_y)$ plane and (ii) the density of states of the π-electrons. The results are compared and contrasted with the earlier results of Coulson on a graphite layer. This model boron layer was then wrapped into a "model boron nanotube". After a discussion concerning chirality and symmetry of these tubes, the electronic properties were discussed within the zone-folding scheme. As to future directions, generalizations which may prove feasible of earlier work by Dancz et al.[15] on a topologically disordered network are proposed.

ACKNOWLEDGMENT

N.H.M. wishes to thank Prof M. P. Tosi and the SNS for much hospitality during a visit to Pisa in 2002. N.H.M. is grateful to the Francqui foundation and in particular to Prof. Dr. Eyckmans for support and motivation. C.A. wishes to acknowledge financial support from Fondi di Ateneo 2002 (University of Pisa). F.E.L. wishes to thank especially Prof. V. Popov and Dr. D. Lamoen for helpful and stimulating discussions.

APPENDIX A: THE QUANTUM NETWORK MODEL

1. Introduction and General Formalism. The idea behind the quantum network (QN) model is extremely simple. One joins each atom to its nearest neighbors and then treats electrons (though quantum mechanically, of course) as though they flowed through 1D wires as in an electrical circuit obeying Kirchoff's Laws at every node. This was first introduced by Pauling,[23] and important later contributions include those of Ruedenberg and Scherr[24] who applied the method systematically to a large group of molecules, Coulson[5] who was the first to apply the method to periodic systems (namely graphene), and Montroll[26] who studied a class of model potentials along the bonds which allow for analytical solutions for the wave functions and the density of states. In particular, these methods have been applied to conjugated systems where one assumes that the σ-electrons form the framework and the delocalized π-electrons move along this network.

If $\phi[j]$ denotes the value of the 1D wave function at the jth node (assuming one has made a suitable numbering of all nodes or atoms) the system of equations one has to solve is given by[26]

$$F(q,\eta)\phi[j] = \sum_{i=1}^{c} \phi[j_i] \quad (A1)$$

where $F(q,\eta)$ is a general form factor which contains information about the (possibly parametrized via η) potential along the bonds, and j_i ($i = 1..c$) denotes the index of the c near neighbor nodes (or atoms).

For free electrons along the network (i.e. no potential along the bonds), one has that

$$F(q,\eta) = c\cos(qa) \tag{A2}$$

where a is the bond length (assumed there is only one), and the energy E is given of course by

$$E = \frac{\hbar^2 q^2}{2m} \tag{A3}$$

For certain specific choices of the potential acting along the bonds, analytic formulas for the structure factor $F(q,\eta)$, the wave functions along the wires, and the resulting DOS can be derived as was shown for instance in the work by Montroll.[26]

For large molecules it is convenient to use the matrix formulation of the problem as was proposed by Ruedenberg and Scherr[24] (to which we refer the interested reader for more details). If we define for a molecule containing N atoms or units the vector

$$\phi = \begin{bmatrix} \phi(1) \\ \phi(2) \\ \dots \\ \dots \\ \phi(N) \end{bmatrix} \tag{A4}$$

we can write eq A1 in the form

$$\mathbf{F}\phi = 0 \tag{A5}$$

where $\mathbf{F}$ is the so-called "connectivity matrix". It is an $N \times N$ matrix, the structure of which can most easily be explained by writing it down for a simple molecule, for instance benzene. If we number all C atoms in a chosen direction from 1 to 6, we obtain for $\mathbf{F}$ the matrix

$$\mathbf{F} = \begin{pmatrix} -F(q,\eta) & 1 & & & & & 1 \\ 1 & -F(q,\eta) & 1 & & & & \\ & 1 & -F(q,\eta) & 1 & & & \\ & & 1 & -F(q,\eta) & 1 & & \\ & & & 1 & -F(q,\eta) & 1 & \\ 1 & & & & 1 & -F(q,\eta) & \end{pmatrix} \tag{A6}$$

where the omitted elements are all zero. The eigenvalues of this matrix, say F_n, then follow from the secular equation

$$|\mathbf{F}| = 0 \tag{A7}$$

combined with eqs A2 and A5 in the case of free electrons or from a generalization of eq A2 in the case of a potential along the bonds.

2. Periodic Systems. For periodic systems eqs A1 or A5 can be considerably simplified. If the vectors $\mathbf{a}_i$ ($i = 1..c$) connect every lattice point to its c nearest neighbors, Bloch's theorem implies that

$$\phi[j_i] = \phi[j]e^{i\mathbf{k}\cdot\mathbf{a}_i} \tag{A8}$$

Then, assuming there is only one atom in the Brillouin zone eq A1 immediately reduces to

$$F(q,\eta) = S(\mathbf{k}) \tag{A9}$$

with the structure factor $S(\mathbf{k})$ given by

$$S(\mathbf{k}) = \sum_{i=1}^{c} e^{i\mathbf{k}\cdot\mathbf{a}_i}$$

and $\mathbf{k}$ is a wave vector of the first Brillouin zone of the periodic structure. For free electrons along the network one immediately obtains for the energy bands $E^{QN}(\mathbf{k})$

$$E^{QN}(\mathbf{k}) = \frac{q^2}{2} = \frac{1}{2}\left\{\frac{1}{a}\cos^{-1}\left(\frac{1}{c}S(\mathbf{k})\right)\right\}^2 \tag{A10}$$

where atomic units have been used. For a more detailed discussion on the use of the Quantum Network model to periodic systems we refer the interested reader to the study of Hoerni.[25]

3. More Recent Related Theories: Use of Feynman Propagators. Let us suppose that at time $t = 0$ (i.e. canonical density matrix analogue, $\beta = it$ where $\beta = (k_B T)^{-1}$, with k_B denoting Boltzmann's constant and T the absolute temperature) the electron can be located at a particular point, say O, on one of the line segments of the tree. The electron wave function on this line segment for $t > 0$ is the free-particle propagator

$$\frac{1}{\sqrt{4\pi it}}e^{iy^2/4t} \tag{A11}$$

where the distance y is to be measured from the initial point O. The electron then diffuses outward from O. As usual in the network model, the wave function is required to vary continuously, but the current divides equally down the remaining $c - 1$ branches, where c denotes the number of nearest neighbors. The wave function ψ and $1/(c-1)$ $\partial\psi/\partial x$ evaluated at the node serve as initial conditions for the wave function itself in the next $c - 1$ segments. These boundary conditions go back to Griffiths.[27] But, as Ringwood stresses, in this situation of an infinite tree the network is simply connected. The same procedure is to be adopted at the next node and so on.

In fact the simplest procedure analytically is to employ the Green function, to be calculated, between two points, say O and P, distanced respectively x and x' from a node. In the initial line segment the Green function takes the form[14]

$$-\frac{1}{2}\frac{1}{\sqrt{-E}}e - \sqrt{-E}|y| \tag{A12}$$

where the energy is taken to be negative, positive energies being obtained by analytic continuation. Putting $\omega = \sqrt{-E}$, the Green function between the two points O and P then

follows as (T denotes Tree)

$$G_T(P, O; E) = (e^{-\omega x'}, e^{\omega x'})\, Z(b_{N-1})Z(b_{N-2})...Z(b_1)Z(x)\begin{pmatrix}\frac{\omega}{2}\\0\end{pmatrix}^{-1} \quad \text{(A13)}$$

where b_i is the length of a segment and $Z(b)$ denotes the matrix

$$\frac{1}{2}(q-1)^{-1}\begin{pmatrix}qe^{-\omega b} & (q-2)e^{\omega b}\\(q-2)e^{-\omega b} & qe^{\omega b}\end{pmatrix} \quad \text{(A14)}$$

The Green function G_L on the lattice (L) is then obtained by a sum over suitable restricted walks (γ)[14] as

$$G_L(x, x';E) = \sum_\gamma e^{i\alpha(\gamma)} G_T(\gamma x, x';E) \quad \text{(A15)}$$

where $\alpha(\gamma)$ enters the phase of the wave function through

$$\psi(\gamma x) = e^{i\alpha(\gamma)}\psi(x) \quad \text{(A16)}$$

Ringwood[14] uses the above results to recover the (more directly calculated) density of states in a graphitic layer given by Coulson.[5]

APPENDIX B: TIGHT BINDING RESULT FOR THE MODEL BORON LATTICE AND RELATION TO THE QN MODEL

For the model boron lattice considered above, we have only 1 atom per unit cell which is assumed to contribute only 1 π-electron. There is thus only one band in the first Brillouin zone. The Bloch orbital corresponding to the translational eigenstate **k** generated by this atom is given by

$$\phi_\pi = \frac{1}{\sqrt{N}}\sum_{i=1}^{N} e^{i\mathbf{k}.\mathbf{R}_j}\varphi_\pi(\mathbf{r}-\mathbf{R}_j) \quad \text{(B1)}$$

where φ_π denotes the atomic π-orbital centered on lattice position $\mathbf{R}_i$ and N the number of atoms in the crystal. The energy $E(\mathbf{k})$ is then given by the secular equation

$$|H - ES| = 0 \quad \text{(B2)}$$

where the matrices H and S are now one-dimensional. If we denote the crystal Hamiltonian (which is assumed to depend only on **r**) by $\hat{H}$ the only matrix element of H, say $\langle H\rangle$, is given by

$$\langle H\rangle = \frac{1}{N_{i,j=1}}\sum^{N} e^{ik.(\mathbf{R}_i-\mathbf{R}_j)}\langle\varphi_\pi(\mathbf{r}-\mathbf{R}_j)|\hat{H}|\varphi_\pi(\mathbf{r}-\mathbf{R}_i)\rangle \quad \text{(B3)}$$

If we now only take into account nearest neighbor interactions this can be rewritten as

$$\langle H\rangle = \frac{1}{N_{i=j=1}}\sum^{N}\epsilon_\pi + \frac{1}{N_{i=j=1}}\sum^{N} e^{ik.(\mathbf{R}_i-\mathbf{R}_j)}\langle\varphi_\pi(\mathbf{r}-\mathbf{R}_j)|\hat{H}|\varphi_\pi(r-\mathbf{R}_i)\rangle \quad \text{(B4)}$$

$$= \epsilon_\pi + \frac{1}{N}\sum_{i=1}^{N}\sum_{j=1}^{N} e^{ik.(\mathbf{a}_j)}\langle\varphi_\pi(\mathbf{r}-(\mathbf{R}_i+\mathbf{a}_j))|\hat{H}|\varphi_\pi(\mathbf{r}-\mathbf{R}_i)\rangle \quad \text{(B5)}$$

$$= \epsilon_\pi + \sum_{j=1}^{c} e^{ik.(\mathbf{a}_j)}\langle\varphi_\pi(\mathbf{r}-(\mathbf{R}_i+\mathbf{a}_j))|\hat{H}|\varphi_\pi(\mathbf{r}-\mathbf{R}_i)\rangle \quad \text{(B6)}$$

where the vectors $\mathbf{a}_j$ connect every lattice position $\mathbf{R}_i$ to its c nearest neighbors and

$$\epsilon_\pi = \langle\varphi_\pi(\mathbf{r})|\hat{H}|\varphi_\pi(\mathbf{r})\rangle$$

For the model boron lattice considered here we then obtain for the energy

$$E^{TB} = \epsilon_\pi + \{[e^{ik.(\mathbf{a}_1)} + e^{-ik.(\mathbf{a}_1)}]t_1 + [e^{ik.(\mathbf{a}_2)} + e^{-ik.(\mathbf{a}_2)}]t_2 + [e^{ik.(\mathbf{a}_3)} + e^{-ik.(\mathbf{a}_3)}]t_3\}$$

$$= \epsilon_\pi + tS(\mathbf{k})$$

with

$$t_i = t = \langle\varphi_\pi(\mathbf{r}-\mathbf{a}_i)|\hat{H}|\varphi_\pi(\mathbf{r})\rangle \qquad i = 1..3 \quad \text{(B7)}$$

since the π-orbitals are symmetric with respect to rotations in the plane and all near-neighbor atoms are at equal distance, and

$$S(\mathbf{k}) = \sum_{j=1}^{c} e^{i\mathbf{k}.(\mathbf{a}_j)}$$

On the other hand from the QN model we obtained (in au)

$$E^{QN}(\mathbf{k}) = \frac{q^2}{2} = \frac{1}{2}\left\{\cos^{-1}\left(\frac{1}{6}S(\mathbf{k})\right)\right\}^2 \quad \text{(B8)}$$

The function

$$f(x) = \frac{1}{2}\{\cos^{-1}(x)\}^2 \quad \text{(B9)}$$

is plotted over its domain [-1, 1] in Figure 10. To obtain correspondence with the tight binding calculation this function should be a linear function with a negative slope. Except very close to the lower boundary, we indeed find a linear behavior for $f(x)$ with a slope of about -1.2 which yields for t the value $-1.2/c$, where c is the near-neighbor coordination number, here equal to 6. The curve has an intersection at about 1.2, which then corresponds to ϵ_π. Clearly, apart from a topological similarity, both methods also exhibit analytical similarities.

APPENDIX C: BORON-NITRIDE SYSTEMS

1. Isolated Benzene and Borazole Levels. The building block of graphene is benzene (without its H atoms: i.e., a

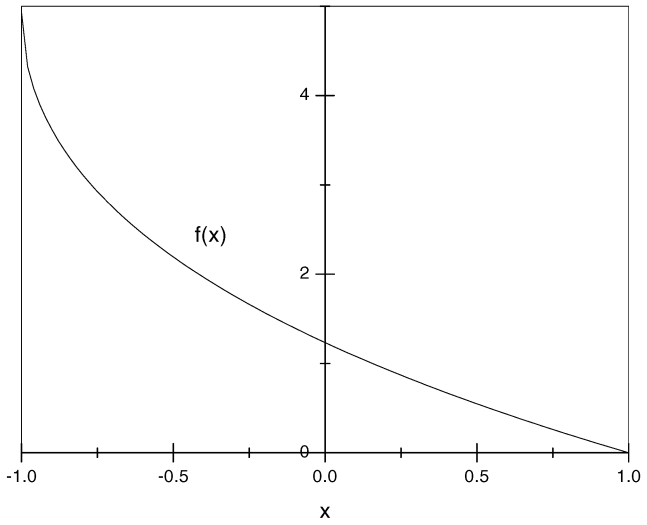

Figure 10. Plot of the function $f(x) = 1/2\{\cos^{-1}(x)\}^2$. To obtain analytic correspondence with the tight binding result we must have a linear relation, and this is found to be true over most of the domain of $f(x)$.

hexagon of C atoms) while for a boron nitride layer it is a hexagon on which B and N atoms alternate. It is natural enough therefore to appeal to a simple treatment of bonding in these two molecules and then to extend the discussion to graphene and a BN layer. Following the survey of one of us[28] we treat in this Appendix benzene and borazole by a common approach to their π-electron level spectrum, following Roothaan and Mulliken.[29] We note that one of the objectives of their study was to treat the ultraviolet spectra of benzene and borazole by the semiempirical molecular orbital method.

Ignoring interactions between neighboring ring atoms, one has for the secular equations for the six molecular orbitals derivable from linear combinations of $2p_\pi$ atomic orbitals of the ring atoms

$$\det\begin{pmatrix} A & 1 & & & & 1 \\ 1 & A & 1 & & & \\ & 1 & A & 1 & & \\ & & 1 & A & 1 & \\ & & & 1 & A & 1 \\ 1 & & & & 1 & A \end{pmatrix} = 0 \text{ (benzene)} \qquad \text{(C1)}$$

where all the omitted elements vanish. Note that this equation is identical to the secular equation obtained from the QN model, and so obviously the structure of the energy spectrum predicted by both methods will be similar.

For borazole we have similarly

$$\det\begin{pmatrix} A' & 1 & & & & 1 \\ 1 & A'' & 1 & & & \\ & 1 & A' & 1 & & \\ & & 1 & A'' & 1 & \\ & & & 1 & A' & 1 \\ 1 & & & & 1 & A'' \end{pmatrix} = 0 \text{ (borazole)} \qquad \text{(C2)}$$

For benzene, for example, A involves not only the desired energy E but also Coulomb and resonance integrals, and the overlap S between adjacent C atoms (appropriate generalization for borazole involves evidently both B and N atomic orbitals).

These secular equations can be reduced (by suitable similarity transformations) to the form

$$\det\begin{pmatrix} A' & 2 & & & & \\ 2 & A'' & 1 & & & \\ & 1 & A' & 1 & & \\ & & 1 & A'' & 1 & \\ & & & 1 & A' & 1 \\ & & & & 1 & A'' \end{pmatrix} = 0 \text{ (borazole)} \qquad \text{(C3)}$$

where, to pass from the borazole result to benzene, one has to set $A' = A'' = A$.

The MOs corresponding to the roots $A = -2$ and $A = -1$ (twice) in benzene, or the corresponding orbitals in borazole, are each doubly occupied in the ground state.

Without going into further details, let us simply state the above in a form such that one can describe the effect of the π-electron eigenvalues of bringing molecules together into a larger compound, the molecular levels then clearly being broadend into bands. To describe this broadening we follow Coulson and Taylor[30] and rewrite the above formulas in an explicit manner for borazole

$$(\alpha_B - E)(\alpha_N - E) - g^2(\beta - ES)^2 = 0 \qquad \text{(C4)}$$

where the Coulomb integrals are denoted by α_B and α_N on boron and nitrogen atoms, respectively, while β denotes the so-called resonance integral.

By way of example, to obtain results for benzene, we merely set $\alpha_B = \alpha_N = \alpha_c$ and then we find discrete allowed values of g^2 (corresponding to discrete values of A above) as $g^2 = 1$ (twice) and $g = 4$. It is to be stressed that the electronegativity difference between B and N will be reflected in the difference between α_B and α_N. The fact that boron is more electronegative than nitrogen is reflected in the inequality $\alpha_B > \alpha_c > \alpha_N$. We have already emphasized in the body of the text that this is a crucial point in highlighting an essential difference between the electronic structure of graphene and of a layer of boron nitride.

2. Broadening of π-Electron Energy Levels into Bands. For details of the tight-binding calculation of graphite,the interested reader must consult the study of Coulson and Taylor.[30] However, the point to be reiterated is that the molecular energy levels, corresponding to discrete values of g^2 quoted above, will be broadend into bands. The detailed nature of the structure of graphene merely gives a spread of values of g^2 that is found to embrace the range 0 to 9 after considerable calculation. Defining sums and differences of Coulomb integrals as

$$E_0 = \frac{1}{2}(\alpha_B + \alpha_N) \qquad \text{(C5)}$$

and

$$\delta = \frac{1}{2}(\alpha_B - \alpha_N) \qquad \text{(C6)}$$

and introducing also $Z = E - E_0$, which merely shift the zero of energy, and $\gamma = \beta - E_0 S$, then one obtains

$$Z = \frac{-2\gamma g^2 S \pm [4\gamma^2 g^4 S^2 + 4(\delta^2 + g^2\gamma^2)(1 - g^2 S^2)]}{2(1 - g^2 S^2)} \qquad \text{(C7)}$$

Denoting the result of adopting the plus sign in eq C7 by $Z_+(g)$, then by allowing g^2 to embrace the range $0-9$ already quoted, it is a straightforward matter to demonstrate that $Z_+(g)$ has its lowest value equal to δ, having a range which is continuous up to a maximum value, while $Z_-(g)$ decreases to its minimum from the value $-\delta$. Thus, for the layer of boron nitride, the π-levels are separated into 2 subbands, with an energy gap 2δ which can be associated directly from the above discussion with the electronegativity difference between B and N. In contrast, for graphene, one must put $\alpha_B = \alpha_N = \alpha_c$ and δ tends to zero. Hence, instead of the (substantial) energy gap ($\sim$4 eV) in the BN layer, in graphene the π-bands touch since $\delta \rightarrow 0$.

REFERENCES AND NOTES

(1) See for instance: March, N. H.; Mucci, J. F. *Chemical Physics of Free molecules*; Plenum Press: New York, 1993; and references therein.
(2) Saito, R.; Dresselhaus, G.; Dresselhaus, M. S. *Physical properties of carbon nanotubes*; Imperial College Press: London, 1998.
(3) Amovilli, C.; March, N. H. *Chem. Phys. Lett.* **2001**, *347*, 459.
(4) Amovilli, C.; Howard, I. A.; Klein, D. J.; March, N. H. *Phys. Rev.* **2002**, *A66*, 013210.
(5) Coulson, C. A. *Proc. Phys. Soc. (London)* **1954**, *A67*, 608; **1955**, *A68*, 1129.
(6) Lundqvist, S.; March, N. H. *Theory of the Inhomogeneous Electron Gas*; Plenum Press: New York, 1983.
(7) Clougherty, D. P.; Zhu, X. *Phys. Rev.* **1997**, *A56*, 632.
(8) Despa, F. *Phys. Rev.* **1998**, *B57*, 7335.
(9) Siringo, F.; Piccitto, G.; Pucci, R. *Phys. Rev.* **1992**, *A46*, 4048.
(10) March, N. H. *Proc. Camb. Phil. Soc.* **1952**, *48*, 665.
(11) Berezin, A. A. *J. Math. Phys.* **1986**, *27*, 1533.
(12) Zhu, H.-Y.; Klein, D. J.; Seitz, W. A.; March, N. H. *Inorg. Chem.* **1995**, *34*, 1381.
(13) Bulusheva, L. G.; Okotrub, A. V.; Boltalina, O. V. *J. Phys. Chem. A* **1999**, *103*, 9922.
(14) Ringwood, G. A. *J. Math. Phys.* **1981**, *22*, 96.
(15) Dancz, J.; Edwards, S. F.; March, N. H. *J. Phys.* **1973**, *C6*, 873.
(16) Boustani, I.; Quandt, A.; Hernández, E.; Rubio, A. *J. Chem. Phys.* **1999**, *110*, 3176.
(17) Boustani, I. *Surf. Sci.* **1997**, *370*, 355.
(18) Saito, R.; Dresselhaus, G.; Dresselhaus, M. S. *Phys. Rev.* **2000**, *B61*, 2981.
(19) Leys, F. E.; Amovilli, C.; Howard, I. A.; March, N. H.; Rubio, A. *J. Phys. Chem. Solids* **2003**, *64*, 1285.
(20) Östling, D.; Tománek, D.; Rosén, A. *Phys. Rev.* **1997**, *B55*, 13980.
(21) Niedenzu, K.; Dawson, J. W. *Boron−nitrogen compounds*; Springer-Verlag: Berlin, 1965.
(22) *Synthesis and properties of boron nitride;* Pouch, J. J., Alterovitz, S. A., Eds.; Trans. Tech Publications: Zurich, 1990.
(23) Pauling, L. *J. Chem. Phys.* **1936**, *4*, 673.
(24) Ruedenberg, K.; Scherr, C. W. *J. Chem. Phys.* **1953**, *21*, 1565. Scherr, C. W. *J. Chem. Phys.* **1953**, *21*, 1582.
(25) Hoerni, J. A. *J. Chem. Phys.* **1961**, *34*, 508.
(26) Montroll, E. W. *J. Math. Phys.* **1970**, *11*, 635.
(27) Griffiths, J. S. *Trans. Faraday Soc.* **1953**, *49*, 345.
(28) March, N. H. In *Polymers, Liquid Crystals and Low-Dimensional Solids*; March, N. H., Tosi, M. P., Eds.; Plenum: New York, 1984; pp 291−334.
(29) Roothaan, C. C. J.; Mulliken, R. S. *J. Chem. Phys.* **1948**, *16*, 118.
(30) Coulson, C. A.; Taylor, R. *Proc. Phys. Soc.* **1952**, *A65*, 815, 834.

CI0200624